RESEARCH ARTICLE

ADVANCED OPTICAL MATERIALS
www.advopticalmat.de

Hierarchical Twist: Chirality Across Scales in Cellulose Cholesterics

*N. Monge, L.F.V. Pinto, E. Ferreira, P.L. Almeida, J.L. Figueirinhas, A.L. Carvalho, P.J. Sebastião, and M.H. Godinho**

One of the unresolved aspects of cellulose-based liquid crystalline phases is their chirality. Although cellulose is intrinsically chiral, both left-handed (LH) and right-handed (RH) chiral nematic phases are reported in cellulose derivatives under different conditions. The origin of these discrepancies—and whether LH and RH twisted structures coexist within a single material—has remained unclear. Here, the first direct evidence of hierarchical LH and RH twisted structures coexisting in a solvent-free, thermotropic cellulose derivative at room temperature is provided. Free-standing cholesteric films exhibit distinct LH and RH twisted domains, whose pitches respond oppositely to uniaxial mechanical strain: the LH pitch increases, while the RH pitch decreases with increasing strain. This contrasting response results from the coexistence of intertwined LH and RH twisted structures, whose optical axes are oriented differently relative to the strain direction. Notably, after stretching beyond their elastic limit, the films spontaneously recover their original shape within minutes. During this recovery, circular dichroism (CD) measurements reveal an increase in RH pitch and a decrease in LH pitch, evidencing reversible, strain-responsive behavior. Multiscale structural characterization confirms the hierarchical chiral organization and its mechanoresponsive nature, providing new insights into the origin of chirality in cellulose-based liquid crystalline materials.

1. Introduction

Chirality in liquid crystalline systems continues to attract the attention of researchers due to its fundamental importance and its relevant role in enabling diverse functional properties, including optical activity, selective molecular recognition, and dynamic mechanical response.[1,2] Cellulose-based liquid crystalline (LC) phases are particularly interesting. As the most abundant biopolymer on Earth, cellulose provides an ideal renewable and sustainable platform for the design of advanced mesomorphic materials.[3,4] Cellulose intrinsic molecular chirality—arising from the stereochemistry of β-D-glucopyranose units—renders cellulose and cellulose derivatives ideal candidates for studying chiral self-assembly at different length scales.

Despite the right-handed (RH) chirality of cellulose macromolecules, cellulose derivatives' liquid crystalline phases display both left-handed (LH) and RH chiral nematic phases under different preparation

N. Monge, L.F.V. Pinto, P.L. Almeida, M.H. Godinho
i3N/CENIMAT
Department of Materials Science
Faculty of Science and Technology
Universidade NOVA de Lisboa
Campus de Caparica, Caparica 2829-516, Portugal
E-mail: mhg@fct.unl.pt

N. Monge
Faculty of Architecture
University of Lisbon, Rua Sá Nogueira, Pólo Universitário
Alto da Ajuda, Lisbon 1349-055, Portugal

The ORCID identification number(s) for the author(s) of this article can be found under https://doi.org/10.1002/adom.202502728

DOI: 10.1002/adom.202502728

N. Monge
Lisbon School of Education
Polytechnic University of Lisbon
Campus de Benfica do IPL, Lisbon 1549-003, Portugal

P.L. Almeida
UniRE e Departamento de Engenharia Mecânica
ISEL – Instituto Superior de Engenharia de Lisboa
Instituto Politécnico de Lisboa
Lisboa 1959-007, Portugal

J.L. Figueirinhas, P.J. Sebastião
CeFEMA & LaPMET and Dept. de Física
IST
Av. Rovisco Pais, Lisbon 1049-001, Portugal

E. Ferreira, A.L. Carvalho
Department of Chemistry
REQUIMTE/UCIBIO and REQUIMTE/CQFB
Faculty of Science and Technology
Universidade NOVA de Lisboa
Campus de Caparica, Caparica 2829-516, Portugal

conditions, including variations in solvent, concentration, or temperature, despite no chiral substituents being added.[5–7] In contrast, cellulose nanocrystals (CNCs), often produced by acidic hydrolysis, are reported to form LH chiral nematic order, a feature attributed to an intrinsic RH twist within the individual nanorods. More recently, this helicity has been attributed to the presence of assembled cellulose nanoparticles, which can act as colloidal chiral dopants.[8,9] The apparent contradiction of having cellulose hierarchical self-assembled structures with different handedness, formed from the same chiral backbone and the same cellulose derivative, has been theoretically justified,[10] but it has nevertheless raised important questions about the fundamental mechanism of chiral amplification in cellulose systems and whether the observed handedness is an emergent property of hierarchical assembly or a direct result of the molecular or nanoscale structural geometry.

In literature, the reflection of both right and left circularly polarized light observed in cholesteric phases obtained from hydroxypropylcellulose (HPC) was attributed to a distortion of the cholesteric helix.[8] A central and unresolved question in the field is whether LH and RH helical domains can coexist within the same cellulose-based LC material. Such coexistence would challenge the traditional view that the chiral nematic pitch is defined by molecular or nanoscale chirality and could suggest the presence of higher-order supramolecular structuring mechanisms. Previous attempts to resolve this issue have been limited by constraints in alignment control, solvent effects, or incomplete structural characterization.

It is also known that the value of the cholesteric pitch of a polymer network can increase or decrease with the application of strain, depending on the orientation of the helix axis.[11] When a mechanical strain is applied perpendicular to the helix axis of the cholesteric phase results in a uniform untwisted configuration results once a critical strain is exceeded, as it removes the distinct, pinned regions of sharp twist. If the strain remains below this threshold, the pitch decreases proportionally with the deformation.[11,12] The unwinding process occurs through conical director configurations when the network is stretched parallel to the helix axis.[13]

In a recent study, the behavior of cholesteric networks under multiaxial mechanical stress was investigated, with a focus on their optical response and chiral structural deformation. The research examined how stretching along different directions—in the same direction, uniaxial, two perpendicular directions (biaxial), and out-of-plane—affects the helical structure and, in turn, the optical properties of the polymer network. The results showed that uniaxial stretching causes a loss of intrinsic circular polarization selectivity due to helix unwinding, while biaxial and out-of-plane stretching preserve this optical function.[14]

In this work, we report the first direct observation of hierarchical coupled left- and right-handed twisted structures within a single solvent-free, thermotropic cellulose derivative system at room temperature. The cellulose derivative chosen enables the precise tuning of mechanical properties and the control of anchoring properties of the cholesteric phase. RH and LH signals were detected by circular dichroism spectroscopy using free-standing films with the optical axis perpendicular to the film surfaces, as confirmed by Polarizing Optical M1.2811icroscopy (POM) working in reflection and transmission modes between cross-polarizers. The controlled stretching of the samples allows the LH and RH domains to exhibit opposing pitch responses, with the LH pitch increasing and the RH pitch decreasing. Scanning electron microscopy revealed that the mesoporous structures templated by the cellulosic films exhibit nanoscale features matching the LH pitch values, supporting the presence of an LH helical arrangement. Furthermore, we show that the presence and interaction of these dual-handed twisted structures contribute to the unconventional shape recovery of the film samples after stretching during strain relaxation. A comprehensive multiscale characterization approach, combining POM, Circular Dichroism (CD), X-ray diffraction images (XRD), small-angle light scattering (SALS), Scanning Electron Microscopy (SEM), and mechanical testing, reveals this unique chiral arrangement's hierarchical and mechanoresponsive nature.

2. Results and Discussion

2.1. Preparation and Characterization of Acetoxypropylcellulose (APC) and Lyotropic Solutions

The cellulose derivative selected, acetoxypropylcellulose (APC) (idealized structure shown in **Figure 1a**) exhibits a cholesteric phase and both thermotropic and lyotropic behavior at room temperature.[15] The APC synthesized for this study forms a liquid crystalline phase at room temperature. The isotropization temperature calculated by POM and DSC is between 110–120 °C, and the glass temperature is below room temperature (≈10 °C) as determined by DSC (Figure S1, Supporting Information). APC also forms lyotropic phases in various solvents, including dimethylacetamide (DMAc). APC was synthesized as a translucent sticky material with a bluish hue (Figure S2a, Supporting Information), with a degree of esterification of 1.28 (Figure S3a,b, Supporting Information). Under cross-polarized light, it exhibits birefringence and, upon shearing, develops defects (Figure 1b.1) that relax slowly over time. When APC is dissolved in DMAc at 55 wt.%, (Figure S2b, Supporting Information) the sheared solution (shear rate equal to $3.5s^{-1}$) exhibits birefringence as observed by POM in transmission mode between cross polars and cross polars and a lambda plate, which within 15 min disappeared, as shown in Figure 1b.2. The dark field observed under cross polars may indicate that the system is isotropic or that the optical axis of the cholesteric phase is perpendicular to the sample substrates. The viscosity versus shear rate curve (Figure 1c) shows that the solution presents rheofluidic behavior, and the presence of the three Onogi and Asada regions[16] confirms the characteristic features of a liquid crystalline regime. Furthermore, the frequency-dependent measurements of the storage (elastic) and loss moduli (Figure 1d) indicate that the solution behaves as a viscoelastic liquid. Based on these rheological measurements and in published results,[17] the relaxed texture observed under crossed polarizers after 15 min (Figure 1b.2) can be attributed to the anchoring of the cholesteric phase with the optical axis quasi-aligned perpendicular to the confining substrates.

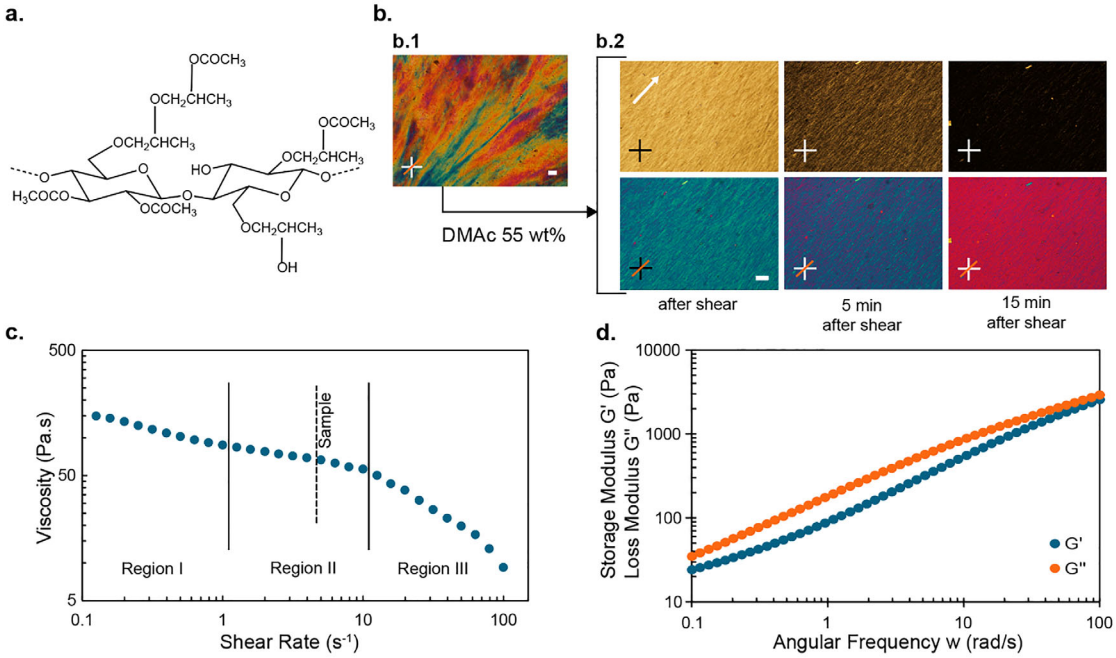

Figure 1. Precursor cellulose-based liquid crystalline materials. a) Idealized structure of acetoxypropylcellulose (APC) with a degree of molar etherification of 2.0, a degree of etherification of 1.5, and a degree of esterification of 2.0. b. Polarized optical microscopy (POM) photos taken in transmission. b.1) Texture of APC, between cross polars and a lambda plate (530 nm), 30 min after shearing. b.2) Textures observed between crossed polars (first row) and between crossed polars with a lambda plate (530 nm) (second row), after shearing a solution of 55 wt.% of APC in dimethylacetamide (DMAc), evolution after shear from 5 to 15 min. c) Viscosity versus shear rate curve for APC/DMAc (55 wt.%) (the shear rate used to make the films is indicated in the graph by "Sample"). d) Loss modulus (G′) and storage modulus (G″) versus angular frequency (ω) for APC/DMAc (55 wt.%). Scale bars: 100 µm (b.1,b.2.).

2.2. Acetoxypropylcellulose Films: Optical and Mechanical Characterization

APC films were prepared from APC/DMAC (Figure S2c, Supporting Information) using a shear casting technique at a shear rate of 4.5 s^{-1}. After solution relaxation and subsequent drying, the resulting films observed by POM appeared dark under crossed polarizers (**Figure** 2a.1). Blue and pink domains are observed when the sample is seen between crossed polarizers and a lambda plate, $\lambda = 530$ nm (Figure 2a.2), indicating that the cellulosic film is not aligned along the shear direction. The APC sample is bluish when seen in reflection (Figure 2a.3), and the CD measurements of the films (Figure 2b) revealed a negative peak indicative of a right-handed helicity, with the helical pitch related to the maximum wavelength of the peak, which appears at 483 nm. The observed characteristics are due to the thermotropic liquid-crystalline behavior of APC at room temperature, the degree of substitution, and the average molecular weight of APC, which are known to influence the material's maximum reflection wavelength.[18]

Through the equation of DeVries $\lambda = \bar{n}\, P cos\theta$, where $\bar{n}$ is the average refractive index, P is the value of the pitch of the cholesteric phase, and θ the angle between the incident beam of light and the optical axis, considering $\bar{n}$ equal to 1.5,[19] the pitch value is of the order of 322 nm. These results are an indication that the twisted cholesteric structure is preserved in the films after relaxation and solvent evaporation, as shown by POM in reflection mode and confirmed by CD spectra. Both reflection and transmission POM imaging suggest that the cholesteric optical axis tends to orient perpendicular to the film surfaces. Due to the sample's liquid viscoelastic nature, SEM imaging proved challenging. Nevertheless, a lamellar structure can be perceived from the SEM image in Figure 2c, which serves to corroborate the cholesteric organisation that is at the origin of the right-handed helicity detected by CD and previously reported for APC samples in the literature.[15]

To better understand the orientation of the optical axis of the cholesteric phase in the soft films, we evaluated their mechanical properties in directions both parallel and perpendicular to the shear direction used during film preparation (stress-strain curves are presented in Figure S4, Supporting Information). Hereafter, the terms "parallel" and "perpendicular" refer to directions relative to the shear-casting direction used during film preparation. The table in Figure 2e shows a summary of the mechanical properties, including Young's modulus and tensile strength. The mechanical properties obtained in this study contrast with those previously reported for APC/DMAc systems, where the cholesteric phase was unwound and the director aligned along the shear direction.[17]

The Young's modulus of the films studied in this work are slightly higher in the parallel direction compared to the perpendicular one (11.18 ± 0.80 MPa vs 7.90 ± 1.50 MPa), and the yield strength and elongation at break are similar in both directions. These slight differences likely arise from the polymer concentration (55 wt.%) and a reduced degree of esterification of APC, which decreases the precursor solution viscosity and promotes

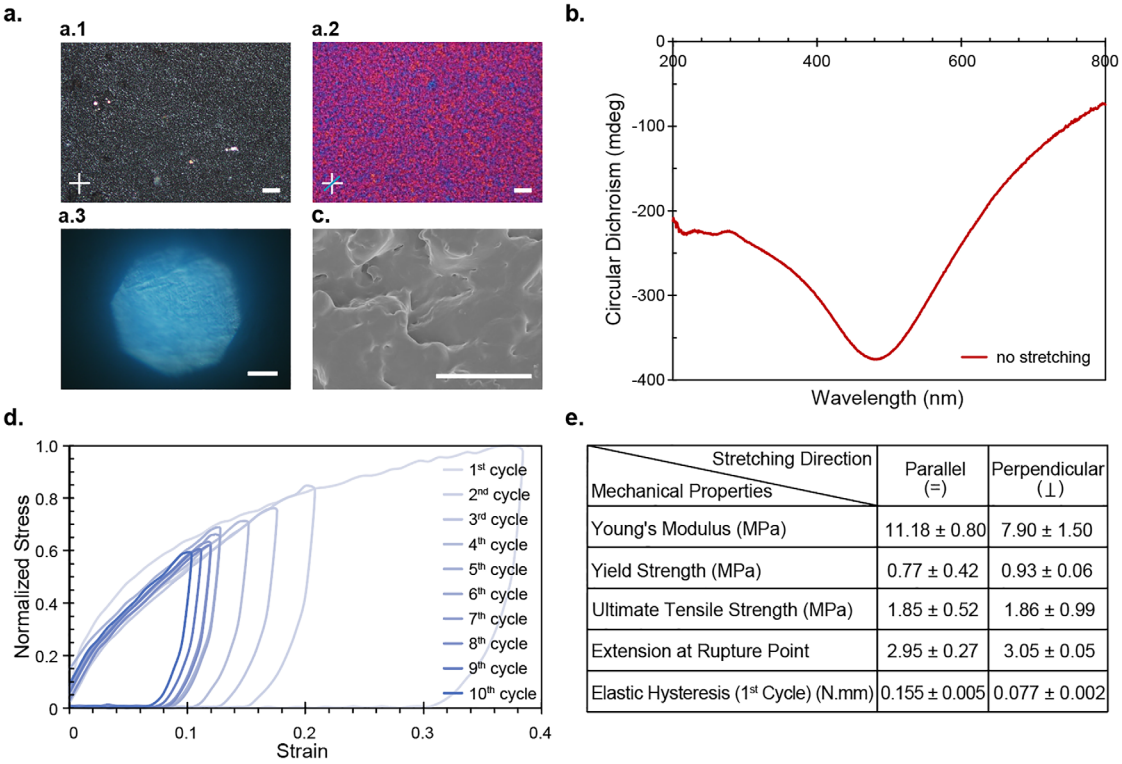

Mechanical Properties \ Stretching Direction	Parallel (=)	Perpendicular (⊥)
Young's Modulus (MPa)	11.18 ± 0.80	7.90 ± 1.50
Yield Strength (MPa)	0.77 ± 0.42	0.93 ± 0.06
Ultimate Tensile Strength (MPa)	1.85 ± 0.52	1.86 ± 0.99
Extension at Rupture Point	2.95 ± 0.27	3.05 ± 0.05
Elastic Hysteresis (1st Cycle) (N.mm)	0.155 ± 0.005	0.077 ± 0.002

Figure 2. Thermotropic acetoxypropylcellulose (APC) films and their structural characterization. a) Polarized optical microscopy (POM) images of the dried film: a.1) acquired in transmission between crossed polars a.2) between cross polars and a 530 nm lambda plate inserted at 45° relative to the cross polarizers a.3 blue color acquired with a POM microscope in reflection mode of the APC sample; b) Circular Dichroism (CD) spectra of the film indicate a right-handed with the maximum wavelength reflected centered at 483 nm. c) Scanning electron microscopy (SEM) photo showing "melted" layers seen perpendicular to the layers surface. d) Normalized stress–strain hysteresis curves for different cycles of APC films cut parallel to the shear direction. Scale bars: 50 µm (a.1, a.2); 100 µm (a.3); 10 µm (c). e) Summary table of mechanical properties for samples cut in parallel and perpendicular directions (Figure S4, Supporting Information).

the relaxation of the liquid crystalline phase during solvent evaporation.

Although the films show comparable strength and ductility in both directions, the higher stiffness along the parallel direction indicates slight mechanical anisotropy. Compared to literature values for shear-aligned cellulose films (15.8 MPa parallel, 39.9 MPa perpendicular[20]), our Young's modulus values are lower and closer between perpendicular and parallel directions, suggesting that the cholesteric structure is largely preserved during shear casting.

Overall, the mechanical tests, combined with POM and CD analysis, indicate that the cholesteric pitch of the order of 322 nm remains with the optical axis predominantly perpendicular to the film surfaces.

The viscoelastic nature of the films was further examined through cyclic tensile testing (Figure 2e). The presence of hysteresis, observed as the area between the loading and unloading curves, indicates partial energy dissipation during deformation, likely due to internal friction and molecular rearrangements within the cholesteric structure. This energy loss was quantified using the loss ratio, defined as the ratio of the hysteresis loop area to the total energy input during loading.

The loss ratio values remained high in both the parallel and perpendicular directions, indicating that the films are mainly viscous (Figure S4, Supporting Information). Since the loss ratios are similar in both directions, these findings support the data obtained from stress-strain curves and the observed optical textures. This confirms that the shear-cast films exhibit viscous elastic behavior after solvent evaporation and that any preferred molecular alignment along the shear direction, which could have been induced during preparation from the precursor solutions, was not retained in the final films.

2.3. Characterization of APC Films under Strain

To investigate the slight structural asymmetry detected in the mechanical measurements and its influence on the optical properties of the films, CD spectra were recorded for films submitted to different values of strains in the perpendicular (**Figure** 3a) and parallel (Figure 3b) directions.

To emphasize the position of the peak maxima rather than their intensity as a function of strain, the results were normalized, as described in the Supplementary Material. Figure S5 (Supporting Information) illustrates the decrease in peak intensity with increasing strain, while the corresponding normalized peaks are shown in Figure 3a.

The peak positions for each stretching value are compiled in the table shown in Figure 3d. Uniaxial stretching results in a gradual decrease of the maximum of the right-handed (RH)

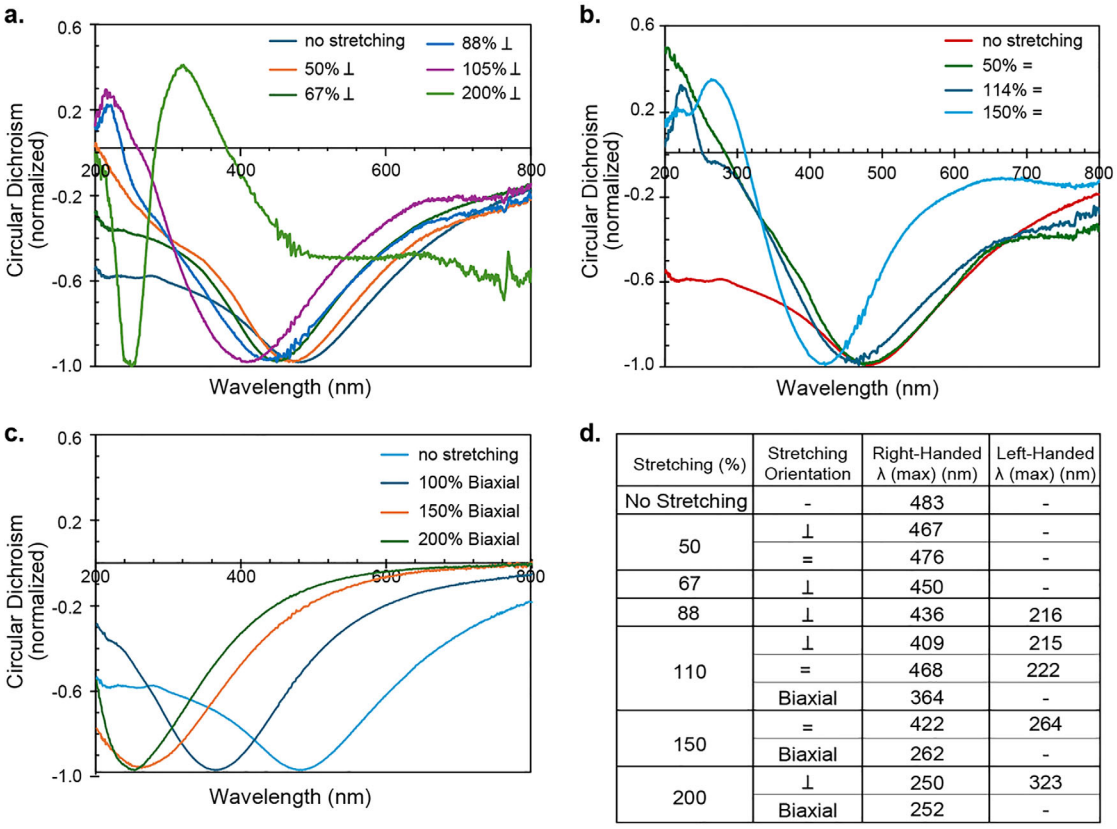

Stretching (%)	Stretching Orientation	Right-Handed λ (max) (nm)	Left-Handed λ (max) (nm)
No Stretching	-	483	-
50	⊥	467	-
	=	476	-
67	⊥	450	-
88	⊥	436	216
110	⊥	409	215
	=	468	222
	Biaxial	364	-
150	=	422	264
	Biaxial	262	-
200	⊥	250	323
	Biaxial	252	-

Figure 3. Revealing dual helicity in cellulose-based liquid crystalline systems. a) Circular dichroism (CD) spectra of uniaxially stretched samples perpendicular to the shear direction, showing a progressive blue-shift of the right-handed (RH) peak and the emergence of a left-handed (LH) peak at shorter wavelengths with increasing strain. b) CD spectra evolution for uniaxially stretched samples parallel to the shear direction reveals similar dual-helicity as perpendicular direction behavior, but with distinct pitch dynamics; the LH peak exhibits a more pronounced shift than the blue shift of the RH peak. c) CD spectra of biaxially stretched samples, no LH signal was detected. d) Summary table of peak positions (λ_{max}) for RH and LH contributions as a function of uniaxial and biaxial stretching.

peaks for both directions, which is an indication of the decrease in the pitch value with increasing strain values. The same behavior was observed for cholesteric elastomers when the cholesteric structure is stretched perpendicular to its optical axis.[21] This reduction in pitch can be associated with a decrease in film thickness (Figure S6, Supporting Information). However, the blue shift of the RH peak is more pronounced in the perpendicular direction ($\Delta\lambda = 74$ nm at 105% strain) than in the parallel direction ($\Delta\lambda = 15$ nm at 114% strain). This behavior can be understood by considering the Young's modulus of the films, which is slightly higher in the parallel direction. This suggests that shear may have induced a tilt of the optical axis along the parallel direction, distinct from that in the perpendicular direction. The observed anisotropy implies that the optical axis of the right-handed (RH) structure becomes slanted in the parallel direction. When the film is stretched along this direction, the tilted RH helices may begin to untwist, counteracting the natural tendency of the film to thin, implying a less reduction of the pitch. In contrast, along the perpendicular direction, untwisting is expected to occur only at higher strain levels. A comparable effect has recently been reported in cholesteric liquid crystalline elastomers.[22]

Surprisingly, a second CD signal emerges at higher strain values, corresponding to a left-handed structure whose maximum peak value increases with strain. Warner et al.[11] state that the pitch of a cholesteric structure increases when stretched along or obliquely to its optical axis. This suggests that an LH structure at an angle to the RH structure may exist and unwind once a certain strain threshold is reached.

Uniaxial stretching is known to lead to a loss of intrinsic circular polarization selectivity due to helix unwinding.[13] Initially, RH structures began to exhibit an LH signal once the applied uniaxial strain exceeded a certain threshold. Due to unwinding of the helix, both RH and LH channels can reflect the same wavelength, indicating loss of intrinsic circular polarization as described.[13,14] However, this trend contrasts with our findings, where increasing strain causes a decrease in the wavelength of the RH peak and an increase in the wavelength of the LH maximum peak. Also, the uniaxial stretching of the films induces an increase in birefringence, accompanied by the appearance of transmission textures under POM resembling oil streaks, which become progressively more distinct with increasing strain, indicating a directional alignment along the stretching direction (Figure S7, Supporting Information).

The CD peaks observed between 200 and 300 nm have also been reported in the literature for cellulose nanofiber composite materials,[23] the authors attributed these peaks to contributions

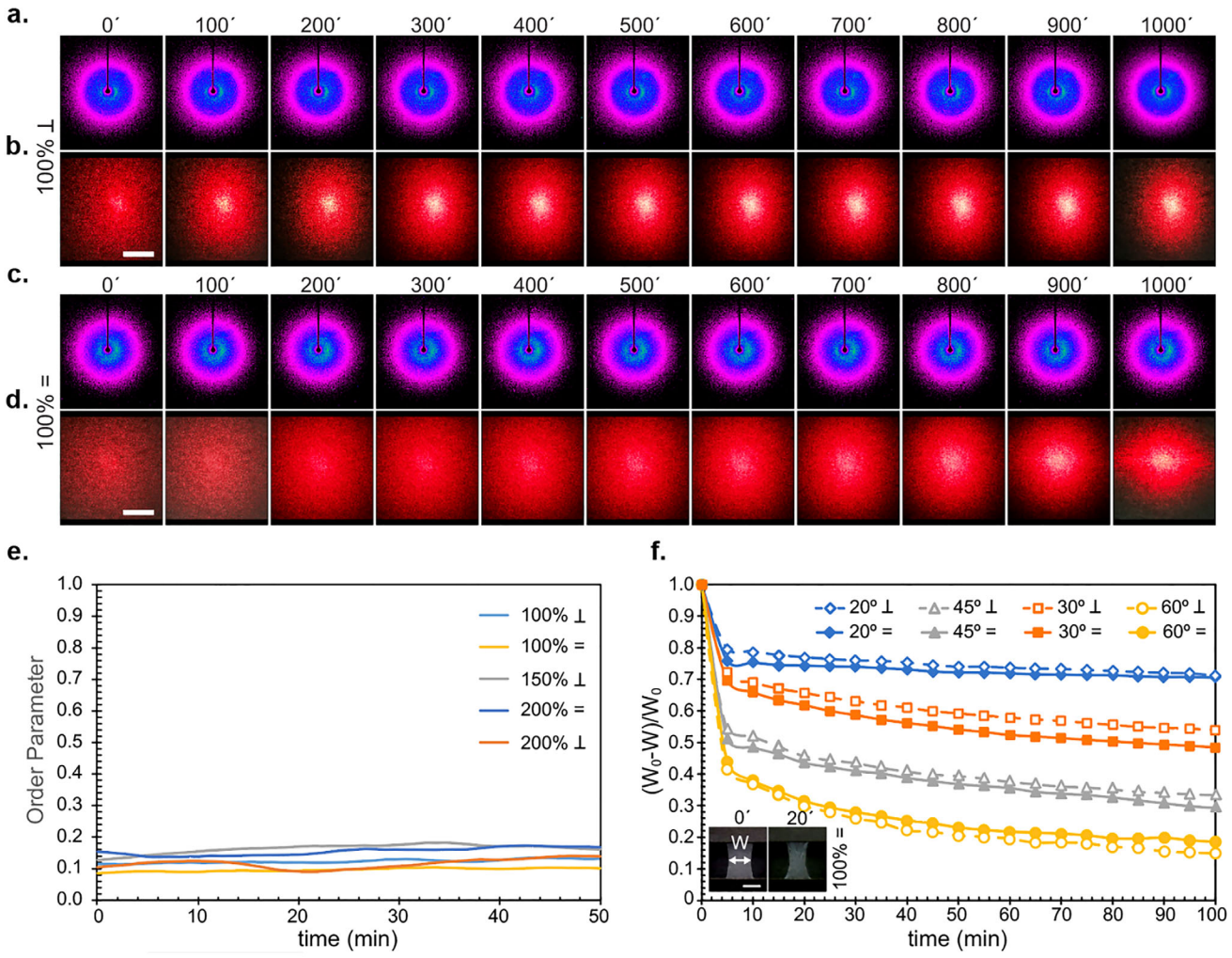

Figure 4. Time evolution of stretched films. a,b) Evolution of X-ray and SALS measurements performed on a sample 100% stretched in the perpendicular direction, respectively. c,d) Evolution of X-ray and SALS images for a sample 100% stretched in the parallel direction, respectively. e) The evolution of the order parameter calculated from XR diffraction patterns for samples stretched to 100%, 150%, and 200% in perpendicular and parallel directions. f) Evolution of the width (w) of the film stretched 100% for different temperatures. The inset shows images of the width evolution for the first 20′ of a film sample 100% stretched in the parallel direction. Scale bars: 5 mm (b,d, and f. inset).

from absorption, scattering, reflection, and the absorbance of individual components. In our case, the absorbance due to cellulose molecules decreases with increasing strain (Figure S8a,b, Supporting Information). Considering these results, the dominant contribution in our system appears to be reflection processes arising from the helicoidal assembly of oriented cellulosic molecules, as both the LH peak wavelength and intensity increase with uniaxial film stretching. Notably, the LH peak shifts under strain to wavelengths beyond the typical cellulose absorbance region (λ = 323 nm for 200% stretching).

We also performed CD measurements on films that were stretched simultaneously in parallel and perpendicular directions (biaxial) (Figure S9, Supporting Information). The results are shown in Figure 3c and summarized in the Figure 3d table. The RH peak shifts to lower wavelength values more rapidly than in uniaxial measurements, and no LH peak is detected. These results can be explained by the fact that the RH blue shift is caused by a greater reduction in film thickness during biaxial stretching. During this process, the LH structure does not achieve directional alignment, which prevents the reinforcement of the CD signal and renders it undetectable.

The effect of temperature was studied by circular dichroism on both relaxed and stretched films. For the relaxed films, it was observed that the maximum peak of the RH structure shifted to higher wavelengths (Figure S8c, Supporting Information). This finding aligns with results reported in the literature for cellulosic liquid-crystalline phases, which indicate an increase in the cholesteric pitch with temperature.[24] For the stretched films, where both length and width were kept constant, the effect of temperature is consistent with the results shown in **Figure 4** of this work, which indicate that, for a fixed length, the film width should decrease as temperature increases. As a result, the film thickness tends to decrease to compensate for the restrictions on width and length that cannot shrink as the temperature

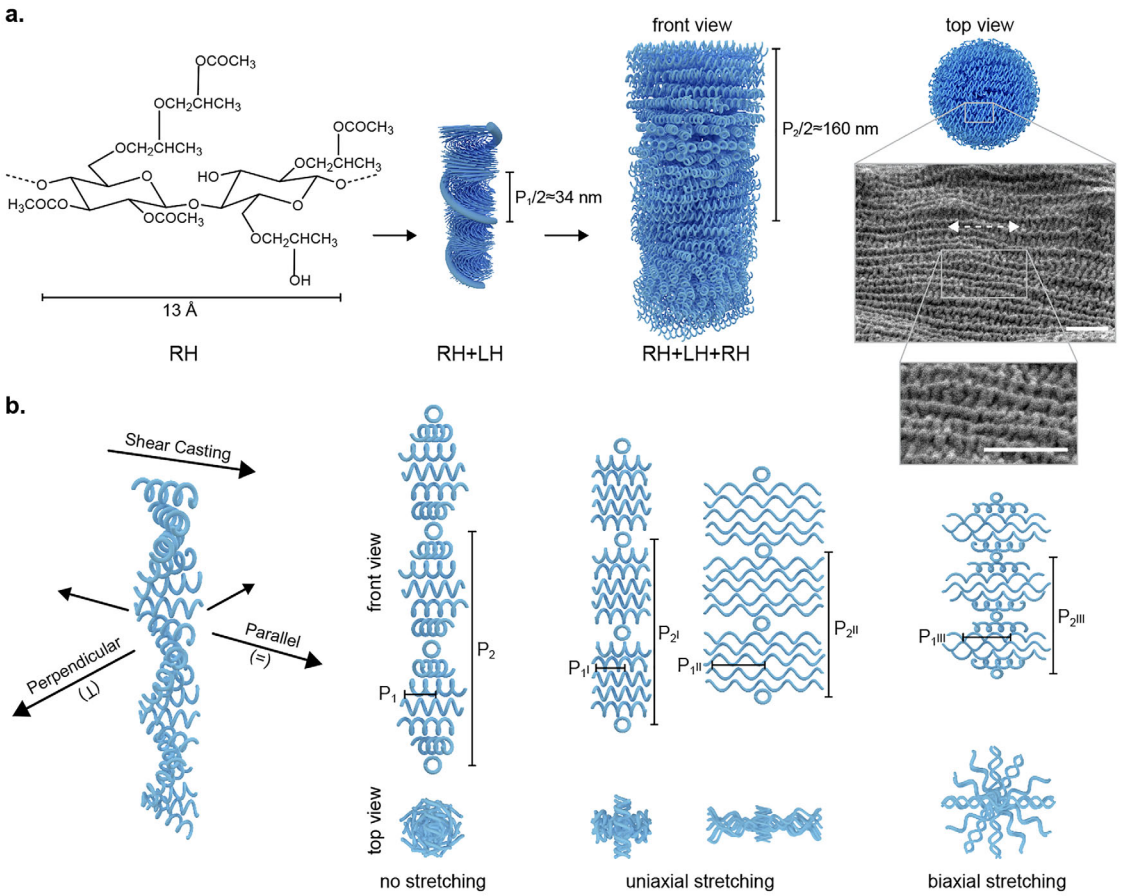

Figure 5. Schematic representations of the hierarchical helical structures and optical changes under uniaxial and biaxial stretching. a) Schematic representation of the coexistence of LH cholesteric structures (pitch P_1) forming RH cholesteric structures (pitch P_2) within the same hierarchical structure, and on the right, top view scheme and corresponding SEM image of the surface of a free-standing mesoporous silica film obtained from the cellulose film (the white dashed double arrow indicates the orientation of the P1 helices.). For simplicity of the schemes, the LH cholesteric structure (with pitch P_1) is represented by an LH helix. b) Simplified helical structures and changes induced by uniaxial and biaxial stretching. Schemes on the left shows unstretched samples, stretching directions and front and top view; schemes in the center show uniaxial stretching, demonstrating the alignment of the LH structures along the stretching direction and increasing of the pitches ($P_{1'}$ and $P_{1''}$) and the unwinding and decreasing of the RH pitches ($P_{2'}$ and $P_{2''}$) upon stretching; scheme on the right illustrates biaxial stretching, showing the reduction of RH pitch ($P_{2'''}$) and the possible increase of the LH pitch ($P_{1'''}$) and no unwinding of RH and LH structures. Scale bar a) 500 nm.

rises, leading to a reduction of the RH pitch structure with increasing temperature. Conversely, the peak related to the LH pitch structure remains unchanged because the sample length is fixed as the temperature increases (Figure S8d, Supporting Information).

Figure 5a presents a diagram illustrating the formation of the hierarchical, self-assembled twisted structures. RH cellulose molecules first organize into LH structures, which then assemble into larger RH structures. The idealized schematic suggests how the pitches of the RH and LH helices become interdependent in the cellulose films under uniaxial deformation—when one increases, the other decreases. For simplicity, the LH twisted structure (pitch P_1), formed by RH-organized cellulose main chain molecules, is depicted as a helix that self-assembles into the RH twisted structure with pitch P_2. Also shown is the top view of the RH twisted (pitch P_2), along with a SEM picture of the free-standing surface of a mesoporous silica film obtained from cellulose liquid crystalline films.

The free-standing mesoporous silica films were prepared by adapting a previously described template-based method,[25] which allows indirect structural analysis of soft matter materials. The films were immersed in tetraethyl orthosilicate (TEOS) aqueous solution and heated at 60 °C for 2 h, followed by drying at room temperature. To remove the cellulose template, the dried films were then calcined at 540 °C in air, resulting in free-standing mesoporous silica films. This high-temperature treatment caused shrinkage of ≈50% of the resulting films.

The surface of the free-standing mesoporous silica films (Figure 5a; Figure S10a, Supporting Information) shows a nanoscale network resembling a "knitted fabric" with features aligned along parallel and oblique directions and spaced at ~34 nm. Although sample preparation may influence the SEM-observed structures, the regular periodicity suggests an ordered origin from the cellulose template. Periodicities below 200 nm are expected in unstretched samples, though they fall below the detection range of CD. The smaller features observed likely

arise from the left-handed (LH) twisted structures and from the shrinkage of the film after template removal. Overall, the surface patterns reflect both the intrinsic periodicity of the cellulose films and the structural changes induced during processing. Previous studies have reported the fabrication of mesoporous silica using liquid crystal templates, noting that while the phase structure was successfully replicated, significant shrinkage of the material also occurred.[26] The cross-section of the mesoporous silica films (Figure S10b, Supporting Information) reveals other periodicities that are attributed to the RH helical structures.

Figure 5b shows a simplified schematic of the RH twisted structure under uniaxial and biaxial stretching. It illustrates how changes at the molecular and nanoscale levels of the LH structure (with pitch P_1) influence the pitch variation of the RH structure (P_2). These diagrams aim to represent the CD and SEM results. Under uniaxial stretching, the helices begin to unwind, and to align the LH helices along the stretching direction, allowing the LH peak to be detected by CD. In contrast, under biaxial stretching, the observed decrease in P_2 is attributed solely to the reduction in film thickness, without helix unwinding and alignment.

To perform the structural characterization of the films under uniaxial stretching X-ray diffraction images and SALS measurements were conducted to monitor the director alignment over time (Figure 4a–d; Figure S11, Supporting Information)

The orientational order parameter ($\langle S \rangle$) (Figure 4e) was calculated from the X-ray diffractograms according to Deutsch:[27]

$$< S >= 1 - N^{-1}\frac{3}{2}\int_0^{\frac{\pi}{2}} I(\phi)\left\{ sin^2(\phi) + \sin(\phi)\, cos^2(\phi)\, ln\left[\frac{(1+\sin\phi)}{\cos\phi}\right]\right\} d\phi \quad (1)$$

with, $N = \int_0^{\frac{\pi}{2}} I(\phi)\, d\phi$, $I(\phi)$ the azimuthal intensity distribution and ϕ the azimuthal angle. The values of the order parameter are very low (they vary between 0.08 and 0.18) and remain nearly constant over time, even at 200% strain. In contrast, SALS measurements reveal a progressive increase in orientational order over time, both in parallel and perpendicular directions. This time-dependent behavior observed by SALS suggests a reorientation of the material under strain, consistent with liquid crystalline flow characteristics. Despite this, the X-ray data confirms that the cholesteric helical structure remains long after stretching. Thus, the increased order detected by SALS is likely due to a gradual reorientation of the cholesteric axis toward the stretching direction. Considering the results obtained from X-ray patterns and SALS as a function of time, the data suggest that the cholesteric axis is, on average, oriented differently depending on the direction of the applied deformation. Initially, the cholesteric axis appears to be more aligned perpendicular to the stretching direction, likely because reorienting it to this configuration involves a lower activation energy compared to aligning it along the parallel direction. However, the distinct evolution of activation energy with increasing strain suggests that the material's internal structure responds differently when deformation is applied parallel or perpendicular to the shear direction used during film casting from the lyotropic solution.

To highlight the differences between the perpendicular and parallel directions of the samples, the width of the films was measured as a function of time and temperature under various imposed strains, while keeping the length constant (Figure 4f; Figure S12, Supporting Information). If the deformation is considered to occur at constant volume, the width decreases slightly more in the parallel direction than in the perpendicular direction, at room temperature. This can be understood by the thickness decrease that can be associated with the decrease of the pitch of the RH helix, which is more pronounced for the perpendicular direction.

2.4. Relaxation of the Films after Stretching

The relaxation behavior of the films was investigated by allowing the material to return to its original shape, as shown in Movies S1 and S2 (Supporting Information) and **Figure 6**. Figure 6a,b. illustrates the reduction in sample length over time for films stretched parallel and perpendicular to the shear direction. The experimental values were fitted to a model equation for liquid viscoelastic fluids $\frac{L}{L_0}(t) = \lambda(t) = \lambda_0 + (\lambda_{\max} - \lambda_0) \times \exp(-\frac{t}{\tau})$, where $L(t)$ is the length (or deformation) of the film at time t, L_0 is the original (undeformed) length of the film, $\lambda(t) = \frac{L}{L_0}(t)$ is the stretch ratio at time t, a dimensionless measure of the deformation, λ_0 is the final (or equilibrium) stretch ratio, λ_{max} is the maximum stretch ratio, i.e., the value of λ at t = 0, immediately after deformation, t is the time after release of the applied stress or strain, and τ is the characteristic relaxation time, describing how fast the material returns to equilibrium. The τ values give evidence that the relaxation time depends upon the initial stretching and the stretching direction for 30% and 50% of initial stretching (30% parallel direction τ = 20 min, perpendicular direction τ = 30 min (Figure S13, Supporting Information) 50% parallel direction τ = 30 min, perpendicular direction τ = 40 min) while for 100% of initial stretching the values for the parallel and perpendicular directions are similar, τ = 207 min. Overall, the trend shows that as the initial stretching increases, the relaxation time also increases. The relaxation of the film can also be followed by CD as seen in Figure 6c. The relaxation of a film initially 88% stretched implies the decrease of the pitch of the LH helix to wavelengths <200 nm and the increase of the pitch of the RH helix to 505 nm, which is much >450 nm found for the sample after stretching and much more similar to the maximum wavelength of the peak before stretching (483 nm). In Figure 6d the sequence of images gives the relaxation of the film toward its initial length after being 100% stretched in the perpendicular direction.

3. Conclusion

In this work, we demonstrate that left- and right-handed structures with distinct pitch values exist within the same cellulose-based liquid crystalline phase. While the presence of both RH and LH structures in cellulosic lyotropic films and solutions has been previously reported—often attributed to cholesteric unwinding or the presence of a birefringent layer between two cholesteric domains of the same handedness[9,28]—our findings suggest a different mechanism. We show that LH and RH structures emerge at different length scales and may be inherently linked in cellulose liquid crystalline phases, such that they cannot be treated as separate entities. Circular dichroism measurements confirm the

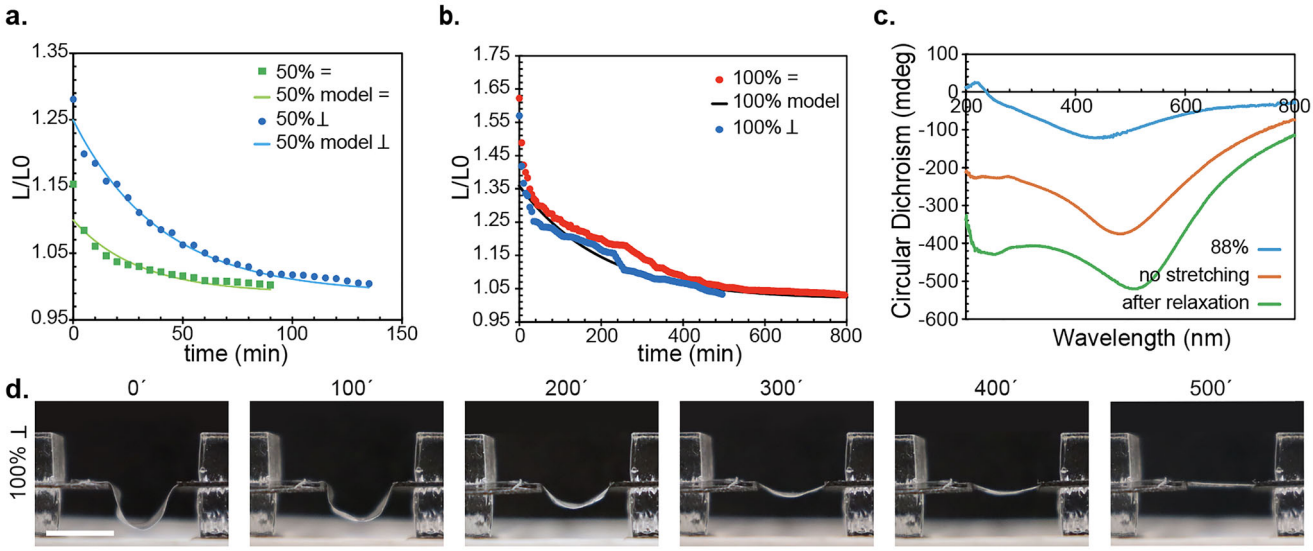

Figure 6. Length relaxation dynamics of stretched APC films. a,b) Relative length reduction of samples stretched in directions parallel and perpendicular to 50% and 100%, respectively. c) CD of APC film prior, during, and after relaxation of APC films. d) Time-lapse images showing shape evolution during relaxation for samples 100% stretched in the perpendicular direction. Scale bar: 5 mm (d).

presence of both chiralities, and mesoporous films derived from free-standing cellulosic liquid crystalline templates further support the existence of the LH phase, revealing spatial features at length scales consistent with LH helical pitch.

Interestingly, under strain, the LH structure exhibits an increase in both pitch and peak intensity, while the RH structure shows a decrease in intensity and shifts to lower wavelengths. Upon release of the strain, the LH peak shifts back to shorter wavelengths and the RH peak shifts to longer wavelengths, with a corresponding increase in intensity. These CD observations occur simultaneously with the unexpected recovery of the film's original dimensions, even after being stretched well beyond the elastic regime.

To rationalize these findings, we propose a dual-helicity model. At the molecular level, cellulose RH chains organize into LH pseudo-layers. These layers, in turn, hierarchically self-assemble into an RH cholesteric superstructure. The LH component, with pitch P_1, defines the local pseudo-layer architecture; the RH component, with pitch P_2, arises from their global stacking. Importantly, P_1 and P_2 are inversely coupled: as P_1 increases, P_2 decreases, and vice versa. Under biaxial deformation, the film thickness decreases more rapidly than under uniaxial deformation, leading to a reduction in the P_2 component, whose optical axis is oriented perpendicular or nearly perpendicular to the film plane. In contrast, the P_1 component is not detected by CD, likely due to its optical axes being distributed within or close to the plane of the film prior to deformation. Our results show that strain determines the balance between these interdependent structures.

Together, these findings reveal an additional level of structural complexity in cellulosic liquid crystals. A simplified framework is proposed to interpret the observed results and the hierarchical organization of right-handed cellulose assemblies. This work brings more questions related to our understanding of cellulose-based hierarchical structures and opens the way for novel applications related to its mechanical and optical behavior.

4. Experimental Section

Statistical Analysis: The quantitative data were presented as the mean, and the sample size was mentioned in the description of the adopted method. The error was estimated by calculating the standard deviation (SD) of the mean and was given as mean ± SD.

Synthesis of (Acetoxypropyl) Cellulose (APC): The synthesis was adapted from Rusig et al.,[24] Tseng et al.,[15] and Costa et al.,[29] as follows: Typically, 50 g of hydroxypropylcellulose (HPC) (Aldrich, nominal $\overline{M_w}$= 100,000 g mol^{-1}, Molar substitution ($\overline{MS}$) = 2.3 (determined by ^{1}H NMR)) is added (portion-wise) to acetic anhydride (160 g) under stirring. To initiate esterification, acetic acid (15 g) is added dropwise at room temperature. The chemical reaction is allowed to proceed for 1 week under stirring at room temperature. The reaction is quenched by adding the homogeneous solution to water, allowing the precipitation of APC. Purification of APC is achieved through sequential precipitations using acetone as the solvent and water as the anti-solvent. Pure APC is dried at 60 °C under vacuum with 75% yield. The characterization of the produced APC was performed by ^{1}H-NMR using $CDCl_3$ as solvent. The calculated Degree of Acetylation of APC was 1.28. Lyotropic solutions of APC 55 wt.% in DMAc can be obtained within weeks by allowing the polymer to fully solubilize at room temperature.

Preparation of the Films: The lyotropic solutions of APC 55 wt.% in DMAc were thoroughly mixed at room temperature and cast onto a Teflon plate using a Gardner casting knife at a controlled speed of 5 mm s^{-1}.[30] The films were allowed to dry at room temperature. The thickness of the dried solid films obtained was 50 ± 2 µm. The films were cut into convenient-sized rectangular pieces with the longest dimension of the sample either along the direction of the casting shear or perpendicular to it.

To obtain the chiral nematic mesoporous silica films, the original casted shear films were immersed in 10 mL of tetraethyl orthosilicate (TEOS) (1.2 mL/5.4 mmol) aqueous solution and maintained at 60 °C for 2 h. Following treatment, the films were removed from the solution and dried at room temperature. Pyrolysis of the cellulose-based films was carried out by initially heating the samples to 100 °C at a rate of 120 °C h^{-1} and holding for 2 h, followed by further heating to 540 °C at the same rate and holding at this temperature for 6 h. After gradual cooling to room temperature, the resulting free-standing mesoporous silica films were recovered.

Polarized Optical Microscopy: All images were acquired using an Olympus BX-51 polarized optical microscope (Olympus Corporation, Tokyo, Japan), equipped with a SCHOTT KL2500 LCD cold light source and coupled with an Olympus DP73 digital camera. Image acquisition was conducted using Olympus Stream Basic software, version 1.9. A Berek compensator coupled to a homemade stretching apparatus was used to measure the birefringence of the films.

Rheology Measurements: The rheological characterization was performed with an Anton Paar MCR 501 rheometer, with a plate/plate geometry of 50 mm in diameter (PP50) and a gap of 1 mm, at room temperature. Frequency sweeps were conducted within a range of 0.1 to 100 rad s^{-1} at 25 °C. Flow curves were carried out between 0.1 and 100 s^{-1} at 25 °C. Two replicas were used for each measurement.

Mechanical Properties: The mechanical properties of thin films were evaluated using uniaxial tensile and mechanical cycling tests. The uniaxial tensile tests were carried out using a Minimat Firmware 3.1 tensile machine (from Rheometric Scientific) equipped with a 20 N load cell. The mechanical cycling tests were performed using a static-dynamic miniature testing machine, model Inspekt Micro LC 100N (from Hegewald & Peschke) equipped with a 10 N load cell. Data was acquired using LabMaster software version 4.2.1.2. All tests were performed at room temperature using a speed of 5 mm min^{-1}. For each measurement, five samples collected by cutting the films in parallel and perpendicular directions were used. The samples had initial lengths of 5 and 2.5 mm and cross sections of ≈ 0.055 mm^2. Biaxial mechanical tests were conducted using custom-built equipment that enabled precise strain control for the acquisition of circular dichroism spectra (Figure S9, Supporting Information).

Small Angle Light Scattering: All samples were mounted on a fixed support positioned 40 cm from the target. A He-Ne laser (model LHP 991, Melles Griot Optical Systems) operating at a wavelength of 632.8 nm with an output power of 1 mW was used as a light source. Image acquisition of the scattering pattern was performed using a CANON EOS R100 digital camera equipped with an RF-S 18–45 mm IS lens. Images were captured every 20 min over a total period of 1000 min, at room temperature.

X-Ray Measurements: X-ray scattering measurements were performed at room temperature using a Bruker D8 Venture diffractometer, equipped with a PHOTON II-70 CMOS 2D detector (pixel size 0.135 mm). The X-ray beam, with a wavelength of 1.54184 Å, was generated by a Diamond IμS Copper anode X-ray tube operated at 50 kV and 1 mA. The thin film samples were mounted on a rectangular support frame and aligned perpendicularly to the incident beam at a fixed sample-to-detector distance of 34 mm. Each exposure was acquired over 30 s, with a total of 50 exposures collected at 20-min intervals throughout the experiment. Diffraction patterns were processed using PROTEUM3 (v6.2.16, 2021) for image integration, and Adxv (v.1.9.14) software was employed for visualization and further order parameter analysis.

Circular Dichroism Measurements: All experiments (film and bulk) were conducted using an Applied Photophysics Chirascan qCD CD spectrometer (Surrey, UK). Samples were analyzed using a demountable quartz cell (type 20C) and the corresponding cell holder, both from Lightpath Optical (Devon, UK). CD spectra were recorded at room temperature over the 200–800 nm wavelength range, with a step size and bandwidth of 1 nm, a scanning rate of 2 nm s^{-1}, and using the low detector target voltage setting. To acquire the CD spectra, the stretched samples were placed between quartz plates (sample holder) to prevent their relaxation during measurements.

Scanning Electron Microscope Images: All images were acquired using a Carl Zeiss AURIGA CrossBeam SEM Workstation (Oberkochen, Germany) equipped with an Oxford energy-dispersive X-ray spectrometer. The in-lens mode was used with an accelerating voltage of 2 kV and a 20 μm aperture size. As preparation for SEM observation, cross-sections of the films, samples were fractured, mounted onto aluminum stubs, and coated with a thin carbon layer using a Q150T ES pumped coater from Quorum (Washington, DC, USA).

Supporting Information

Supporting Information is available from the Wiley Online Library or from the author.

Acknowledgements

This work has been supported by the ERC H2020 Synergy grant 101167171 (ALCEMIST), FCT – Fundação para a Ciência e a Tecnologia, I.P., in the scope of the projects LA/P/0037/2020, UIDP/50025/2020, and UIDB/50025/2020 of the Associate Laboratory Institute of Nanostructures, Nanomodelling and Nanofabrication i3N. European Cooperation in Science and Technology (COST) Action understanding interaction light – biological surfaces: the possibility for new electronic materials and devices (PhoBioS, CA21159). The authors gratefully acknowledge the valuable, inspiring, and insightful discussions with Randall Kamien and Frank Giesselmann.

Conflict of Interest

The authors declare no conflict of interest.

Author Contributions

M.H.G. supervised and directed this project. N.M. and L.F.V.P. prepared the samples and performed their characterization, E.F. made circular dichroism measurements, M.H.G., L.F.V.P., J.L.F., and E.F. analyzed the CD data. N.M. and A.L.C. performed the X-ray measurements, J.L.F. and M.H.G. performed the analysis of the X-ray and SALS data. P.L.A. performed the analysis of the mechanical measurements data. M.H.G. made SEM and POM measurements. M.H.G., J.L.F., P.J.S., and L.F.V.P. contributed to the interpretation of the CD and SEM results. M.H.G. wrote the manuscript, and all authors contributed to its improvement and editing.

Data Availability Statement

The data that support the findings of this study are available from the corresponding author upon reasonable request.

Keywords

chiral nematic liquid crystals, hierarchical twisted supramolecular structures, mechanoresponsive materials, thermotropic cellulose derivatives

Received: August 19, 2025
Revised: September 22, 2025
Published online: October 24, 2025

[1] T. J. White, D. J. Broer, *Nature Mater* **2015**, *14*, 1087.
[2] H. K. Bisoyi, Q. Li, *Chem. Rev.* **2022**, *122*, 4887.
[3] A. P. C. Almeida, J. P. Canejo, S. N. Fernandes, C. Echeverria, P. L. Almeida, M. H. Godinho, *Adv. Mater.* **2018**, *30*, 1703655.
[4] X. Li, J. Liu, X. Zhang, *Adv. Funct. Mater.* **2023**, *33*, 2306208.
[5] J. X. Guo, D. G. Gray, *Macromolecules* **1989**, *22*, 2082.
[6] J. X. Guo, D. G. Gray, *Macromolecules* **1989**, *22*, 2086.
[7] D. G. Gray, in *Cellulose Science and Technology*, John Wiley & Sons, Ltd., Hoboken, **2018**, pp. 253–261.

[8] C. L. C. Chan, M. M. Bay, G. Jacucci, R. Vadrucci, C. A. Williams, G. T. van de Kerkhof, R. M. Parker, K. Vynck, B. Frka-Petesic, S. Vignolini, *Adv. Mater.* **2019**, *31*, 1905151.
[9] B. Frka-Petesic, G. Kamita, G. Guidetti, S. Vignolini, *Phys. Rev. Mater.* **2019**, *3*, 045601.
[10] A. B. Harris, R. D. Kamien, T. C. Lubensky, *Rev. Mod. Phys.* **1999**, *71*, 1745.
[11] Y. Mao, E. M. Terentjev, M. Warner, *Phys. Rev. E* **2001**, *64*, 041803.
[12] P. Cicuta, A. R. Tajbakhsh, E. M. Terentjev, *Phys. Rev. E* **2004**, *70*, 011703.
[13] M. Warner, E. M. Terentjev, R. B. Meyer, Y. Mao, *Phys. Rev. Lett.* **2000**, *85*, 2320.
[14] C. Kwon, S. Nam, S. H. Han, S. S. Choi, *Adv. Funct. Mater.* **2023**, *33*, 2304506.
[15] S.-L. Tseng, A. Valente, D. G. Gray, *Macromolecules* **1981**, *14*, 715.
[16] S. Onogi, T. Asada, in *Rheology: Principles*, 1st Ed, (Eds.: G. Astarita, G. Marrucci, and L. Nicolais), Springer US, Boston, MA **1980**, p. 127.
[17] M. H. Godinho, D. Filip, I. Costa, A.-L. Carvalho, J. L. Figueirinhas, E. M. Terentjev, *Cellulose* **2009**, *16*, 199.
[18] G. V. Laivins, P. Sixou, D. G. Gray, *J. Polym. Sci., Part B: Polym. Phys.* **1986**, *24*, 2779.
[19] T. A. Trezza, J. M. Krochta, *J. Appl. Polym. Sci.* **2001**, *79*, 2221.
[20] P. L. Almeida, S. Kundu, D. Beja, J. Fonseca, J. L. Figueirinhas, M. H. Godinho, *Cellulose* **2009**, *16*, 427.
[21] C. H. Barty-King, M. Burgonse, S. Vignolini, J. Baumberg, M. De Volder, *Adv. Mater.* **2025**, 2418880.
[22] J. Choi, Y. Choi, J.-H. Lee, M. C. Kim, S. Park, K. Hyun, K. M. Lee, T.-H. Yoon, S. Ahn, *Adv. Funct. Mater.* **2024**, *34*, 2310658.
[23] R. Mujica, A. Augustine, M. Pauly, Y. Battie, G. Decher, V. L. Houérou, O. Felix, *Adv. Mater.* **2024**, *36*, 2401742.
[24] I. Rusig, J. Dedier, C. Filliatre, M. H. Godhino, L. Varichon, P. Sixou, *J. Polym. Sci., Part A: Polym. Chem.* **1992**, *30*, 895.
[25] K. E. Shopsowitz, H. Qi, W. Y. Hamad, M. J. MacLachlan, *Nature* **2010**, *468*, 422.
[26] J. R. Bruckner, J. Bauhof, J. Gebhardt, A.-K. Beurer, Y. Traa, F. Giesselmann, *J. Phys. Chem. B* **2021**, *125*, 3197.
[27] M. Deutsch, *Phys. Rev. A* **1991**, *44*, 8264.
[28] S. N. Fernandes, P. L. Almeida, N. Monge, L. E. Aguirre, D. Reis, C. L. P. de Oliveira, A. M. F. Neto, P. Pieranski, M. H. Godinho, *Adv. Mater.* **2017**, *29*, 1603560.
[29] I. Costa, D. Filip, J. Figueirinhas, M. Godinho, *Carbohydr. Polym.* **2007**, *68*, 159.
[30] M. H. Godinho, J. G. Fonseca, A. C. Ribeiro, L. V. Melo, P. Brogueira, *Macromolecules* **2002**, *35*, 5932.